Denoising based on noise parameter estimation in speckled OCT images using neural network

Article *in* Proceedings of SPIE - The International Society for Optical Engineering · December 2008

DOI: 10.1117/12.814937

Denoising based on noise parameter estimation in speckled OCT images using neural network

Mohammad R. N. Avanaki*[a], P. Philippe Laissue[a], Adrian G. Podoleanu[b] and Ali Hojjat[a]

[a] Kent Institute of Medicine and Health Sciences, University of Kent, Canterbury, CT2 7PD, United Kingdom
[b] Applied Optics Group, School of Physical Sciences, University of Kent, Canterbury, CT2 7NH, United Kingdom

ABSTRACT

This paper presents a neural network based technique to denoise speckled images in optical coherence tomography (OCT). Speckle noise is modeled as Rayleigh distribution, and the neural network estimates the noise parameter, sigma. Twenty features from each image are used as input for training the neural network, and the sigma value is the single output of the network. The certainty of the trained network was more than 91 percent. The promising image results were assessed with three No-Reference metrics, with the Signal-to-Noise ratio of the denoised image being considerably increased.

Keywords: Optical Coherence Tomography (OCT), Neural Network, Speckle Noise Reduction, No-Reference (NR) metrics

1. INTRODUCTION

Optical Coherence Tomography (OCT) is a high resolution, non-invasive imaging modality using non-ionising optical radiation. OCT images are constructed by measuring the time delay and magnitude of optical echoes at different transverse positions [1]. OCT is based on low-coherence interferometry, which uses the spatial and temporal coherence properties of optical waves backscattered from biological tissue [2]. Like other imaging technique based on detection of coherent waves, OCT images are subjected to significant presence of speckle noise. Development of successful speckle noise reduction algorithms for OCT is particularly challenging. Many methods have been proposed to reduce noise in OCT. They include hardware modifications of the OCT system design [2] and application of image processing like locally adaptive filtering [3, 4], soft thresholding of the wavelet subbands with various configurations [3, 5, 6], and averaging in time and frequency domain [7].

In this study, speckle noise is approximated as multiplicative Rayleigh noise, based on speckle statistics by Bashkansky and Reintjes [3]. While an additive noise component exists as well [1], made up of shot noise, light intensity noise, and electronic noise in OCT imaging systems, it may be ignored because it is significantly small compared to the multiplicative speckle noise [8].

* mn96@kent.ac.uk; phone 0044 (0) 122 7782-7940

1st Canterbury Workshop on Optical Coherence Tomography and Adaptive Optics
edited by Adrian Podoleanu, Proc. of SPIE Vol. 7139, 71390E · © 2008 SPIE
CCC code: 0277-786X/08/$18 · doi: 10.1117/12.814937

Here we developed a neural network based noise-parameter-estimator which estimates sigma for Rayleigh noise in each input image. The inverse Rayleigh function with this sigma is then applied to the noisy image, resulting in a reconstructed image without noise.

2. MATERIAL AND METHODS

2.1. Speckle noise in OCT images

Each surface has a special scattering function which represents the population of sub-resolution scatterers being imaged. When a coherent source illuminates an object that is of the same scale or smaller than the wavelength of the source, the interference of the many partial waves in the reflected light, with their random amplitudes and phases, produces a phenomenon known as speckle [8]. There are two main types of scattering: Diffuse scattering, which mainly leads to speckle in the image, and coherent scattering, which creates clear light and dark features [1]. Each of the diffuse scatterers contributes a component to the echo signal in a sum which has a zero mean, two-dimensional Gaussian probability density function (PDF). Envelope detection removes the phase component and so creates an unwanted signal which can be modeled by Rayleigh amplitude PDF [8]. The effect of this signal on each pixel in the image is given by Equation 1.

$$f(x_{i,j}) = \frac{x_{i,j} e^{\frac{-x^2_{i,j}}{2\sigma^2}}}{\sigma^2} \quad \textbf{(1)}$$

Where $x_{i,j}$ is an image pixel and sigma (σ) is noise variance in the image.

Speckle reduces the performance of image segmentation and pattern recognition algorithms that are used to extract, analyze, and recognize diagnostically relevant features. But while speckle as such is unwanted, it also contains useful clinical information about tissue characteristics. Thus, accurate modeling of speckle noise is of paramount importance. To this aim, an artificial neural network (ANN) was used, as the effectiveness of this approach for noise parameter estimation has been demonstrated previously [9, 10].

2.2. Neural network scheme

An Artificial Neural Network (ANN) which comprises a large amount of neurons connecting each other is an intelligent information processing model working in a similar fashion to biological nervous systems.

For a given application, the critical aspects of designing an ANN is choosing an appropriate network size, which consists of the number of layers, the number of nodes per layer connected to each other, training function, learning function and performance function [11]. The configuration of our algorithm which was used to estimate the Rayleigh noise parameter is shown in Figure 1.

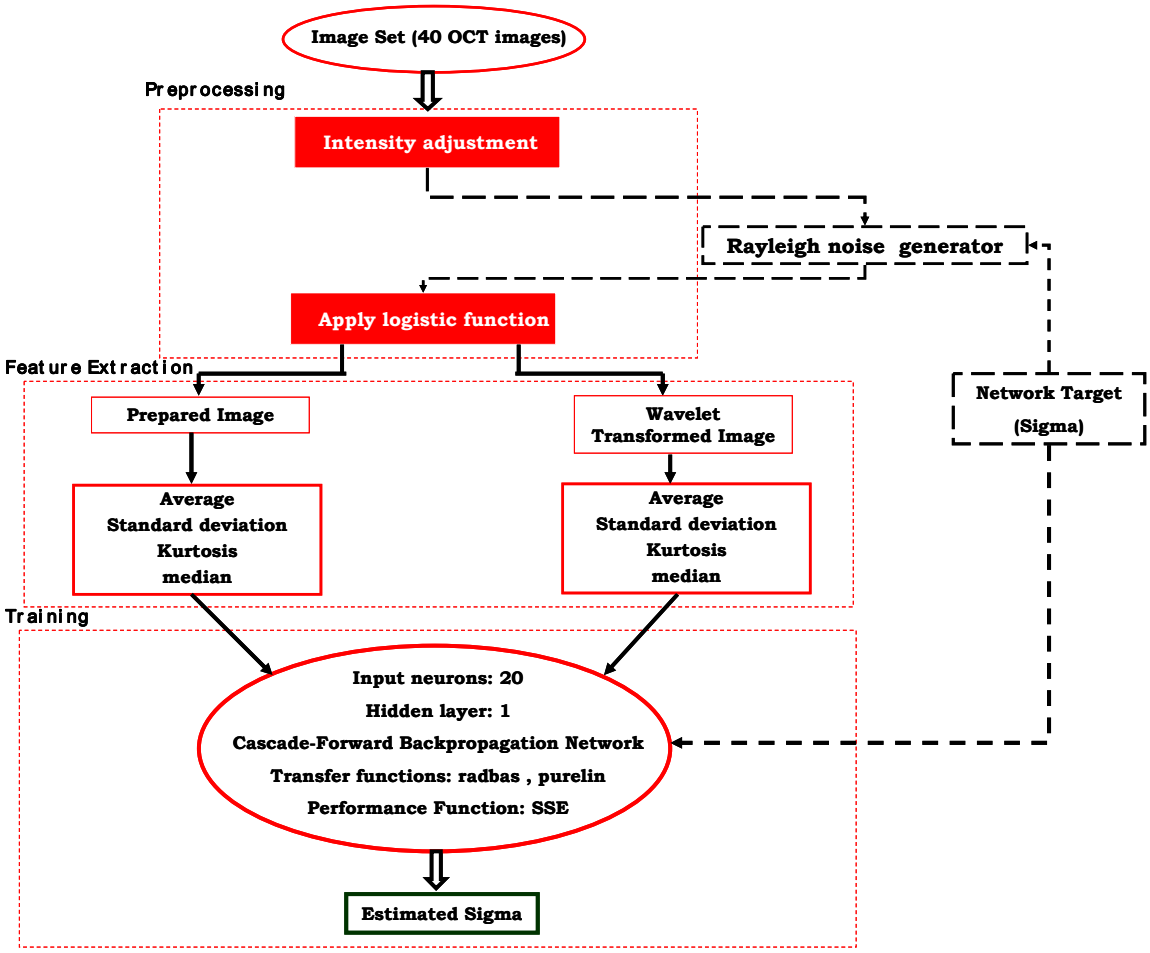

Fig. 1. Schematic diagram of our noise parameter estimator engine (Dotted boxes are used during training)

The algorithm consists of three steps: Preprocessing, feature extraction, and neural network training. The preprocessing is done to make images in the same scale and intensity range. The logistic function is used to convert multiplicative noise into additive noise. In the next stage, a set of twenty features are extracted from the images. The features consist of the image's mean, standard deviation, kurtosis, and median gray scale values. The features were calculated on the original image as well as on wavelet transformed images. The formulae which have been used for mean, standard deviation, and kurtosis are given in the following equations:

$$\mu = \frac{1}{MN} \cdot \sum_{i}^{M} \sum_{j}^{N} x_{i,j} \tag{2}$$

$$\kappa = MN \frac{\sum_{i=1}^{M} \sum_{j=1}^{N} (x_{i,j} - \mu)^4}{(\sum_{i=1}^{M} \sum_{j=1}^{N} (x_{i,j} - \mu)^2)^2} \tag{3}$$

$$\sigma = \sqrt{\frac{1}{MN} \sum_{i=1}^{M} \sum_{j=1}^{N} (x_{i,j} - \mu)^2} \tag{4}$$

Where $x_{i,j}$ indicates the image pixel, and M and N are image dimensions.

The last stage of the algorithm consists of a cascade-forward back propagation neural network. The neural network is similar to a feed-forward network, but includes a weight connection from the input to each layer, and from each layer to the successive layers. For example a three-layer network has connections from layer 1 to layers 2, layer 2 to layer 3, and layer 1 to layer 3. The three-layer network also has connections from the input to all three layers. These additional connections improve the speed at which the network learns the desired relationship [12]. The number of neurons in input layer is 20 with one hidden layer, however, various configurations i.e. three, four, five hidden layers with different numbers of input neurons were tested. The transfer function calculates a layer's output from its input. After testing several transfer functions the combination of Radial Basis Transfer Function and Linear Transfer Function were found to be the best suited for this purpose [13]. In the Figure 2 the employed transfer functions are given.

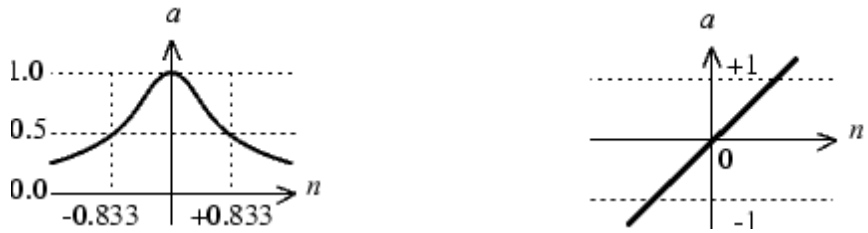

(a) **(b)**

Fig. 2. Transfer Functions, (a) Radial Basis (b) Linear. (*n* is the input-axis, *a* is the output-axis)

With the sum squared error performance function, the network was trained better. Resilent and Hebb functions with the decay weight learning rule are utilized for learning and training, respectively [13].

Forty images acquired with a high resolution OCT system have been utilized to train the neural network. After preprocessing, Rayleigh noise was added to each image (see Figure 1). To allow comprehensive training, various sigmas ranging from 7 to 208 were used; the selected sigmas were obtained by trial and step size of one is used because of discrete changes in gray scale value. By now 8000 images are generated (200 sigmas x 40 images) as a training image set. Twenty statistical features for each image and its wavelet components have been extracted as training input for the neural network. The network is then trained to build the sigma estimator engine.

Training was done with one half of the 8000 images and tested with the other, resulting in 91 percent reliability. The expected sigma against obtained sigma acquired from the trained network for the range of 8 to 207 for 4000 images are drawn in Figure 3.

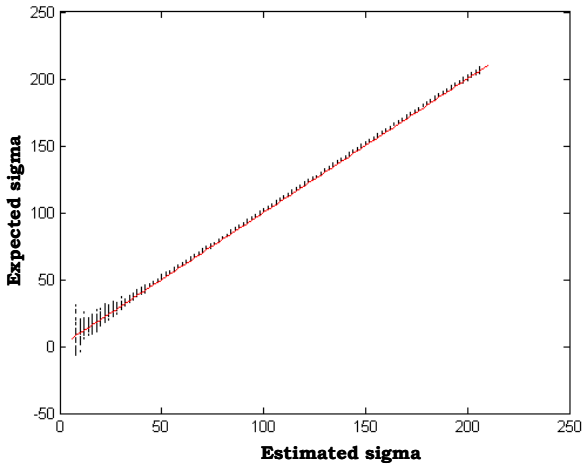

Fig. 3. Expected sigma versus acquired sigma from the neural network (the red line shows the true values)

As seen in Figure 3, the neural network can estimate sigma for values above 45 perfectly. The error for lower values is higher, however, in practice, sigmas with a low value occur very rarely.

Using the trained neural network, we design a full system for denoising OCT images. Figure 4 shows the whole procedure of the approach.

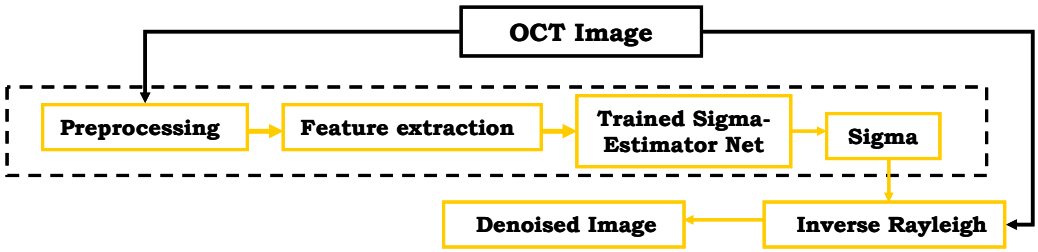

Fig. 4. Full block-diagram of image denoising with neural network

The input image is preprocessed, which consists only of intensity adjustment and applying logistic function. After feature extraction, sigma is then estimated by the trained neural network. Next, an inverse Rayleigh image is generated using the noisy image and the estimated sigma. The inverse-Rayleigh function has been solved numerically; in Equation (1), 2550 values for x (from 0.1 to 255 with the step of 0.1) with various values of sigma (from 8 to 207) have been recorded in a lookup table (2550x200 values). Then, for each of the noisy pixels, the appropriate x value of the lookup table according to the estimated sigma is chosen as a denoised pixel.

3. RESULTS AND DISCUSSION

The algorithm was tested on twenty OCT images of dental implants. The visual results of three test images with fine structures and large areas of noise are presented in Figure 5. The neural network is very effective at removing mid-range

noise. The remaining salt-and-pepper noise was then easily removed using 3x3 median filtering, which is most appropriate for this kind of noise [15]. To compare the effect of 3x3 median filtering itself, we include images processed in only this way. This demonstrates that combining the neural network approach with median filtering produces significantly denoised images with highly preserved edges.

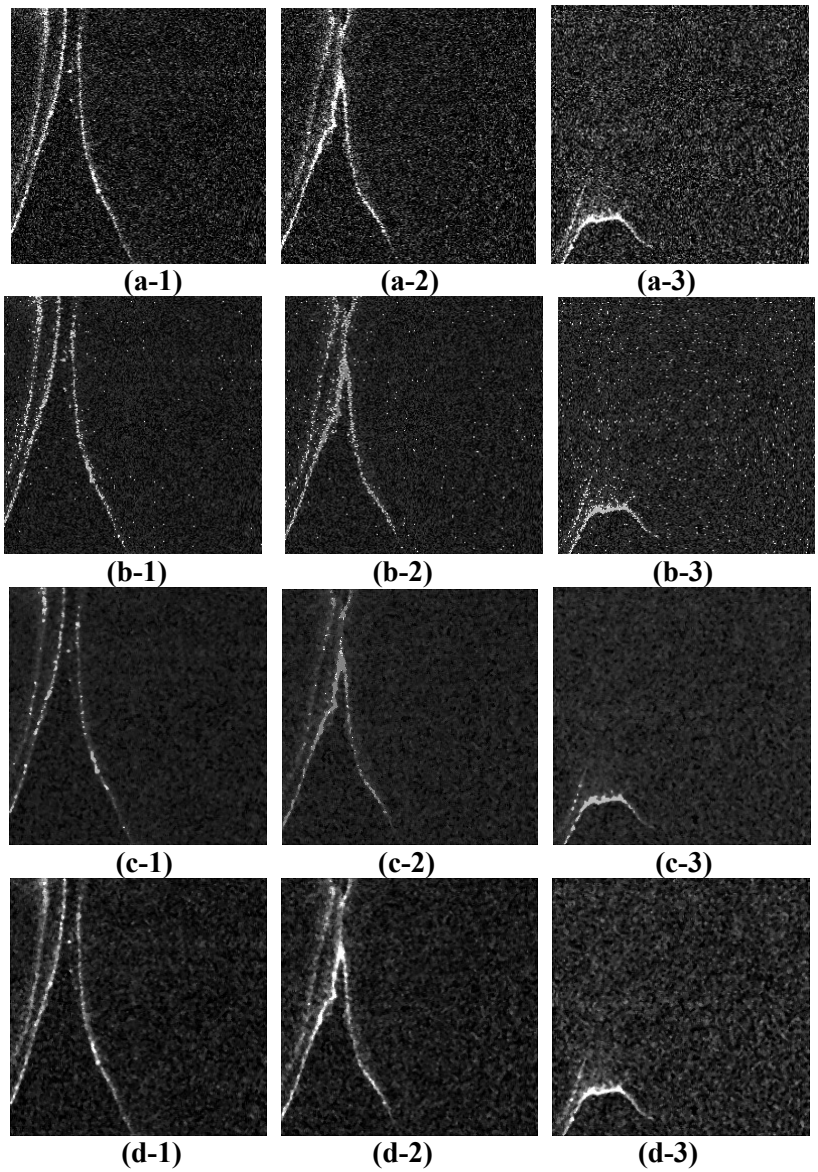

Fig. 5. Application of neural network approach to three OCT noisy images, (a) original test images (b) images denoised with neural network (c) images denoised with neural network followed by 3x3 median filtering (d) images denoised with 3x3 median filter

In addition to single images, image sequences were also processed. We used a z-stack of a dental implant with a defect. 3D projections hereof are shown in Figure 6. The best result is again achieved by combining the neural network with median filtering (third image from left). The contrast is markedly increased, with a high conservation of detail, enabling the dental implant defect to be clearly discerned.

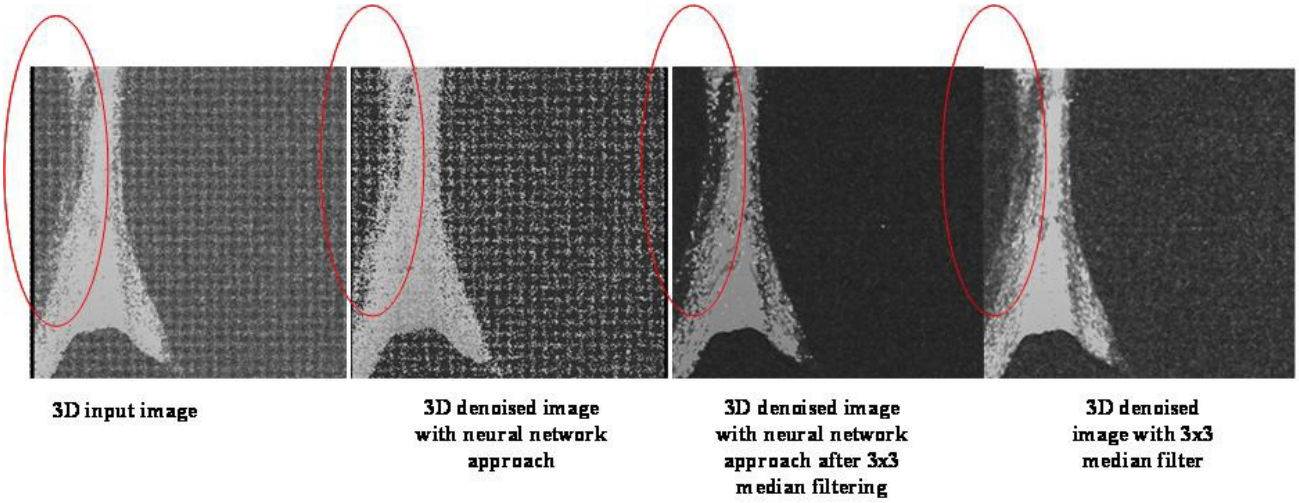

Fig. 6. 3D projection of an OCT image sequence of a dental implant, before and after denoising

As we do not have the noise-free images, we measured the quality of the denoised images using the no-reference quality metrics. The metrics include Signal-to-Noise Ratio (SNR), Contrast-to-Noise Ratio (CNR) and Equivalent Number of Looks (ENL) [11 and 15]. The smoothness of a homogenous region of interest is measured by ENL, and CNR is a measure between an interested area of image rather than the whole image. The image quality metrics definitions are given in Equations 5 to 7 [15].

$$ENL = \frac{1}{H}\left(\sum_{h=1}^{H}\frac{\mu_h^{\,2}}{\sigma_h^{\,2}}\right) \tag{5}$$

$$SNR = 10\log_{10}\left(\frac{\max(I^2)}{\sigma_h^{\,2}}\right) \tag{6}$$

$$CNR = \frac{1}{R}\left(\sum_{r=1}^{R}\frac{(\mu_r - \mu_b)}{\sqrt{\sigma_r^{\,2} + \sigma_b^{\,2}}}\right) \tag{7}$$

Where $\mu_h^{\,2}$ and $\sigma_h^{\,2}$ in ENL represents the mean and variance of the h_{th} homogenous region of interests respectively. I and $\sigma_n^{\,2}$ in SNR represent the linear magnitude image and the variance of the background noise region in the linear magnitude image respectively. μ_b and $\sigma_b^{\,2}$ in CNR represents the mean and variance of the same background noise region as in SNR and μ_r and $\sigma_r^{\,2}$ represents the mean and variance of the r_{th} region of interest which includes the homogeneous regions as well [15].

SNR, CNR, and ENL were calculated for the 20 images (Figure 7). As the graphs show, the SNR and ENL for denoised images are significantly increased using the neural network approach, and are further improved by median filtering. Interestingly, CNR measurements show a slightly weaker performance for our denoising algorithm combined with the median filtering when compared to median filtering alone. This effect was however not discernible upon visual inspection of the images.

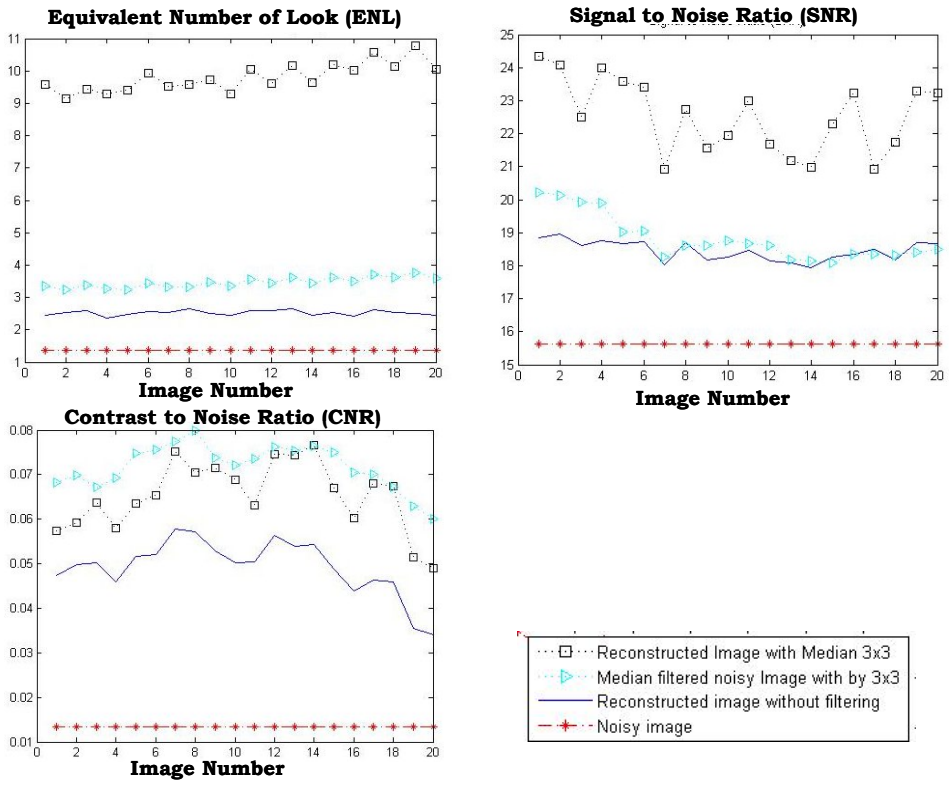

Fig. 7. Numerical assessment of image denoising using SNR, CNR, and ENL metrics. For all three graphs, measurements are shown for the original image (asterisk), the image denoised and reconstructed with either the neural network (line) or processed with 3x3 median filtering (triangle) or both approaches combined (square).

4. CONCLUSION

In this paper, a neural network based noise-parameter-estimator was designed to estimate the sigma for multiplicative Rayleigh noise. This design is based on the assumption that speckle noise is a multiplicative noise with a distribution similar to the Rayleigh distribution function. Moreover, intelligent denoising has been used because speckle in addition to having noise component, also carries useful information about the morphology of the imaged object. The reliability of the trained network was more than 91 percent. The algorithm, tested on 20 images, shows good results, which can be further improved by median filtering. Consequentially, noise is drastically reduced while detail is well preserved, and the SNR of the resultant images is raised by more than 8 dB on average.

ACKNOWLEDGEMENTS

We would like to thank Costas Sirlantzis from the Electronics department for giving advice about neural network, and Cosmin Sinescu of the Victor Babes University of Timisoara who is collaborating with the School of Physical Sciences at the University of Kent, for providing the dental implant images

REFERENCES

[1] Podoleanu, A. Gh., “Optical coherence tomography”, British Journal of Radiology, vol. 78, 935, 976–988, (2005)

[2] Ozcan, A., Bilenca, A., Desjardins, A. E., Bouma, B. E., and Tearney, G. J., "Speckle reduction in optical coherence tomography images using digital filtering", J. Opt. 24, 1901-1910, (2007)

[3] Bashkansky, M. and Reintjes, J., "Statistics and reduction of speckle in optical coherence tomography", Opt. Lett. 25, 545-547, 2000

[4] Rogowska, J. and Brezinski, M. E., "Evaluation of the adaptive speckle suppression filter for coronary optical coherence tomography imaging ", IEEE Trans. Med. Imaging, 19, 1261–6, (2000)

[5] Adler, D. C., Ko, T. H., and Fujimoto, J. G., "Speckle reduction in optical coherence tomography images by use of a spatially adaptive wavelet filter", Opt. Lett. 29, 2878–2880, (2004)

[6] Zlokolica, V., Jovanov, Lj., Pizurica, A., Philips, W.,"Wavelet-based denoising for 3D OCT images", in SPIE Simposium Optical Engineering and Applications, 6696, 123-131, (2007)

[7] Sander, B. Larsen, M., Thrane, L., Hougaard, J. L. and Jørgensen, T. M., "Enhanced optical coherence tomography imaging by multiple scan averaging ", Br. J. Ophthalmol. 89, 207-212, (2004)

[8] Anderson, M. and Trahey, G., "A seminar on k-space applied to medical ultrasound", Web publication, Department of Biomedical Engineering, Duke University, (2006)

[9] Schioler, H. and Kulczycki, P., "Neural Network for Estimating Conditional Distributions", IEEE Trans. Neural Networks, 8, 1015-1025, (1997)

[10] Williams, P. M., "Using Neural Networks to Model Conditional Multi-variate Densities ", Neural Computation, 8, 843-854, (1996)

[11] Avanaki, Mohammad. R. N. and Ebrahimpour, R., "In-service video quality measurements in optical fiber links based on neural network", vol. 17, 5, 415-504, Neural Network World, (2007)

[12] Simoncelli, E. P., "Bayesian Denoising of Visual Images in the Wavelet Domain", Bayesian Inference in Wavelet-Based Model, P. Muller et al., Springer-Verlag New York, 291-308, (1999)

[13] Cinar, Ö., Hasar, H. and Kinaci, C., "Modeling of submerged membrane bioreactor treating cheese whey wastewater by artificial neural network", J Biotechnol, 123, 204-209, (2006)

[14] Bishop, C.M., "Neural Networks for Pattern Recognition", Oxford University Press, Oxford, (1995)

[15] Lim, Jae S., "Two-Dimensional Signal and Image Processing", Englewood Cliffs, NJ, Prentice Hall, 469-476, (1990)

[16] Marks, D. L., Ralston, T. S., and Boppart, S. A., "Speckle reduction by I-divergence regularization in optical coherence tomography", J. Opt. Soc. Am. A 22, 2366–2371, (2005)